Available online at www.sciencedirect.com
ScienceDirect
Journal of the European Ceramic Society 30 (2010) 3253–3258
www.elsevier.com/locate/jeurceramsoc

Spark plasma sintering of HfB_2 with low additions of silicides of molybdenum and tantalum

D. Sciti [a], G. Bonnefont [b], G. Fantozzi [b], L. Silvestroni [a,*]

[a] *CNR-ISTEC, Institute of Science and Technology for Ceramics, Via Granarolo 64, I-48018 Faenza, Italy*
[b] *Université de Lyon, INSA-Lyon, MATEIS CNRS UMR 5510, Bâtiment Blaise Pascal 7, avenue Jean Capelle, 69621 Villeurbanne Cedex, France*

Received 22 January 2010; received in revised form 3 June 2010; accepted 15 June 2010
Available online 16 July 2010

Abstract

HfB_2-based composites containing 3 vol% silicides of molybdenum or tantalum as sintering additives are densified by spark plasma sintering at 1900–2000 °C. Mechanical properties are measured up to 1500 °C in air. 4-pt Flexural strength values at 1500 °C are 480 MPa (64% of the RT value) for the $MoSi_2$-doped composite and 290 MPa (49% of the RT value) for the $TaSi_2$-doped composite. The fracture toughness is insensitive to the temperature change and reaches 5 MPa $m^{1/2}$ for the $TaSi_2$-doped ceramic.

Keywords: Hafnium boride; Spark plasma sintering; Microstructure; Mechanical properties

1. Introduction

Hafnium diboride (HfB_2) has a number of unique properties including hardness, high thermal and electrical conductivity and chemical stability.[1–9] This compound belongs to a family of materials defined as ultra high-temperature ceramics (UHTC) and is considered a valuable candidate for a variety of high-temperature structural applications, such as leading edges and nose caps in hypersonic re-entry space vehicles, rocket nozzle inserts and air-augmented propulsion system components.[1–9] Other applications which benefit from these properties are cutting tools, refractory linings, electrodes and microelectronics. Due to high melting points and low self-diffusion coefficients, sintering of HfB_2 needs pressure-assisted procedures at temperatures of the order of 2000 °C or even higher.[1–9] Moreover, the unavoidable presence of surface oxides, such as B_2O_3 and HfO_2, constitutes an additional factor which hinders the densification of these ceramics. One promising approach for improving the densification is the use of field-assisted sintering techniques, as rapid heating rates may prevent grain coarsening and electrical discharge may favour removal of undesired surface oxides. Recently, much attention has been focused on Spark Plasma Sintering (SPS) which employs a pulsed DC current to activate and improve sintering kinetics.[10–16] In nearly all the reported investigations on the SPS, higher heating rates, lower sintering temperatures and shorter dwelling times have been used in comparison with conventional sintering techniques (hot-pressing, pressureless sintering, etc.). As a result, higher densities, refined microstructures, clean grain boundaries and elimination of surface impurities have been reported which, in turn, determine an overall improvement in the materials performance.[10–16]

This work is focused on the processing, spark plasma sintering and characterization of HfB_2-based composites. Silicides of molybdenum or tantalum are added to HfB_2 as sintering additives in amount of 3 vol%. The addition of silicides of Mo, Ta, Zr has been proved to be very effective in enhancing the densification and the mechanical properties even at high temperature of several boride matrices, including TiB_2, ZrB_2 and HfB_2.[17–21] In addition, as silica-forming compounds, they should offer significant improvement to the oxidation behavior.

Preliminary studies have been carried out to investigate the effect of addition of $MoSi_2$ between 0 and 10 vol% on spark plasma sintered HfB_2.[19–21] The results indicate that in the range investigated, 3 vol% of $MoSi_2$ was the best doping level in order to accomplish a dense refined microstructure and the highest value of room temperature strength tested in 3-pt bending (~780 MPa[19]). However, at that stage a complete characterization was not possible due to limited size of the produced samples.

* Corresponding author.
E-mail address: laura.silvestroni@istec.cnr.it (L. Silvestroni).

0955-2219/$ – see front matter © 2010 Elsevier Ltd. All rights reserved.
doi:10.1016/j.jeurceramsoc.2010.06.006

Table 1
Sintering parameters of the SPS tests for the HBM3 and HBT3 composites.

Sample	Diameter (mm)	Temperature (°C)	Dwell time (min)	Pressure (MPa)	Density (g/cm^3)	Rel. density (%)
HBM3	20	1750	3	75	8.30	75.2
	20	1800	3	75	10.70	97.0
	20	1900	3	75	10.67	96.7
	40[a]	1900	3	80	10.70	98.0
HBT3	20	1750	3	75	8.21	73.8
	20	1900	3	75	8.69	78.1
	20	2000	3	75	10.56	94.9
	30	1900	3	75	9.96	89.5
	30[a]	2000	3	80	10.72	96.3

[a] Sample selected for mechanical characterization.

In this work, HfB_2-based composites containing 3 vol% $MoSi_2$ are fully characterized from mechanical and microstructural point of view. For comparison 3 vol% $TaSi_2$-doped HfB_2 was also produced and characterized.

2. Experimental

The following compositions were prepared from commercial powders:

$HfB_2 + 3\,vol\%MoSi_2$(HBM3)

$HfB_2 + 3\,vol\%TaSi_2$(HBT3)

The characteristics of the starting powders are as follows: HfB_2 (Cerac Incorporated, Milwaukee, USA), −325 mesh, particle size range 0.5–5.0 μm, mean particle size ∼1 μm (by SEM analysis), impurities: Al (0.07%), Fe (0.01%), Zr (0.47%), $MoSi_2$ (Aldrich, Germany), <2 μm, mean particle size 2.8 μm and oxygen content 1 wt%; $TaSi_2$ (ABCR, GmbH & Co, Karlsruhe, Germany), −45 μm. The powder mixtures were ultrasonically treated, ball-milled for 24 h in absolute ethanol using zirconia milling media, subsequently dried in a rotary evaporator and sieved through a 150 μm-mesh screen size. The powder mixtures were sintered in a graphite mould using a SPS equipment (FCT, HPD25). A layer of graphite blanket was placed around the die in order to minimize the heat loss. The temperature was measured by an optical pyrometer focused on the upper punch. The sintering pellets were 40 mm in diameter for HBM3 and 30 mm in diameter for HBT3 and 10 mm in height. The sintering cycle was adopted as follows:

- HBM3, from room temperature up to 1900 °C the heating rate was set at 100 °C/min, a pressure of 80 MPa was applied at room temperature and the holding time was 3 min.
- HBT3, from room temperature up to 1400 °C the heating rate was set at 200 °C/min. At 600 °C, a pressure of 80 MPa was applied. From 1400 °C to the final sintering temperature of 2000 °C the heating rate was decreased to 100 °C/min; the holding time was 3 min.

Bulk densities were measured by the Archimedes method. Relative densities were determined as the ratio between bulk and theoretical densities calculated on the basis of starting nominal compositions using the rule of mixture. Crystalline phases were identified by X-ray diffraction (Siemens D500, Karlsruhe, Germany). The microstructures were analyzed using scanning electron microscopy (SEM, Cambridge S360, Cambridge, UK) and energy dispersive spectroscopy (EDS, INCA Energy 300, Oxford instruments, UK). To this purpose, sample sections were cut from the sintered pellets in the plane parallel to the direction of applied pressure and then polished with diamond paste down to 0.25 μm. Microstructural parameters were determined through image analysis on SEM micrographs of polished surfaces (Image Pro-plus 4.5.1, Media Cybernetics, Silver Springs MD, USA).

Vickers microhardness (HV1.0) was measured with a load of 9.81 N, using a Zwick 3212 tester. Young's modulus (E) was measured by the resonance frequency method on 28 mm × 8 mm × 0.8 mm specimens using a HP gain-phase analyzer. Fracture toughness (K_{Ic}) was evaluated using chevron-notched beams (CNB) in flexure. The test bars, 25 mm × 2 mm × 2.5 mm (length × width × thickness, respectively), were notched with a 0.1-mm thick diamond saw; the chevron-notch tip depth and average side length were about 0.12 and 0.80 of the bar thickness, respectively. The specimens were fractured using a semi-articulated silicon carbide four-point fixture with a lower span of 20 mm and an upper span of 10 mm using a screw-driven load frame (Instron mod.

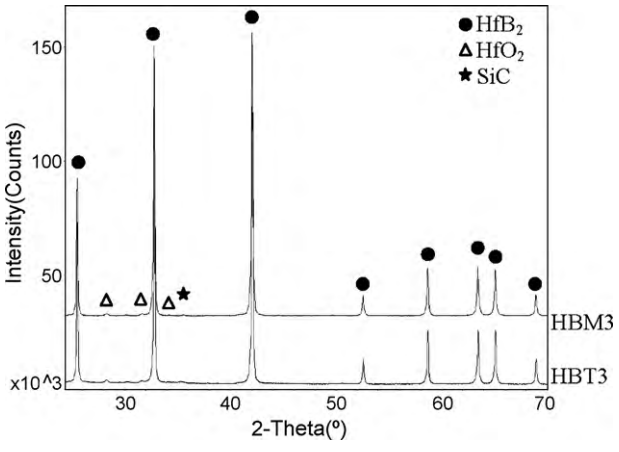

Fig. 1. X-ray diffraction spectra of the two HfB_2-based composites as labeled.

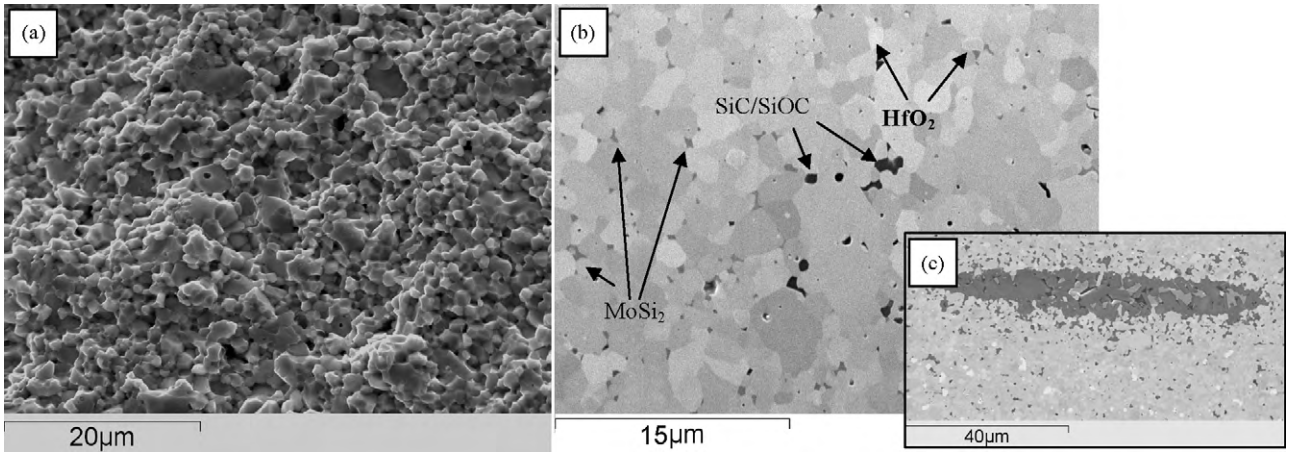

Fig. 2. Fracture surface (a) and polished section (b) of HBM3 composite. An example of SiC agglomerate in (c).

6025). The specimens, three for each composite, were loaded with a crosshead speed of 0.05 mm/min. The "slice model" equation of Munz et al.[22] was used to calculate K_{Ic}. On the same machine and with the same fixture, the flexural strength (σ) was measured at room temperature, 1200 and 1500 °C in air on chamfered bars 25 mm × 2.5 mm × 2 mm (length × width × thickness, respectively), using a crosshead speed of 0.5 mm/min. For the high-temperature tests, a soaking time of 18 min was set to reach thermal equilibrium. Five specimens were tested at room temperature, three at 1200 and 1500 °C.

3. Results and discussion

3.1. Densification behavior

In order to optimize the sintering cycle, preliminary densification tests were conducted on small pellets (diameter 2 cm, height 5 mm), as indicated in Table 1.

For the HBM3 composite, the highest density (10.7 g/cm^3) was achieved at 1900 °C. This value corresponds to a relative density of 98% of the theoretical value.

The compositions with 3% of $TaSi_2$, namely HBT3, required higher temperatures for achieving a good level of densification. The highest bulk density, 10.7 g/cm^3, was obtained at 2000 °C and corresponded to a relative density of 96.4%. It was also found that increasing the $TaSi_2$ amount from 3 to 6 vol%, fully dense materials could be obtained at 1900 °C (not shown in Table 1).

3.2. Microstructural features

3.2.1. HBM3

According to X-ray diffraction illustrated in Fig. 1, besides HfB_2, traces of HfO_2 and SiC were detected as crystalline phases present after sintering. No $MoSi_2$ phase was detected. The polished sections of the composition with $MoSi_2$ are presented in Fig. 2. Little or no porosity was generally found in this sample, which exhibited a fine-grained microstructure. No grain growth occurred during sintering as the resulting mean grain size is about 1 μm, *i.e.* close to that of the starting particles of the HfB_2 powder. Residual pockets of $MoSi_2$ were observed in the microstructure, Fig. 2b. A considerable quantity of HfO_2 (4 vol%) was detected by EDS analysis, which accounts for oxygen contamination of the starting powder,

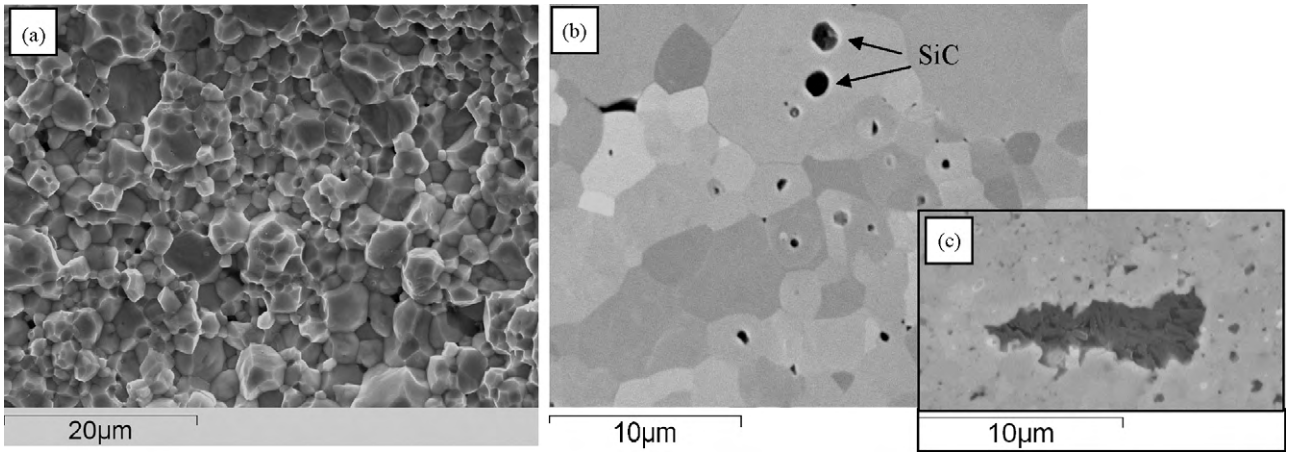

Fig. 3. Fracture surface (a) and polished section (b) of HBT3 composite. An example of SiC agglomerate in (c).

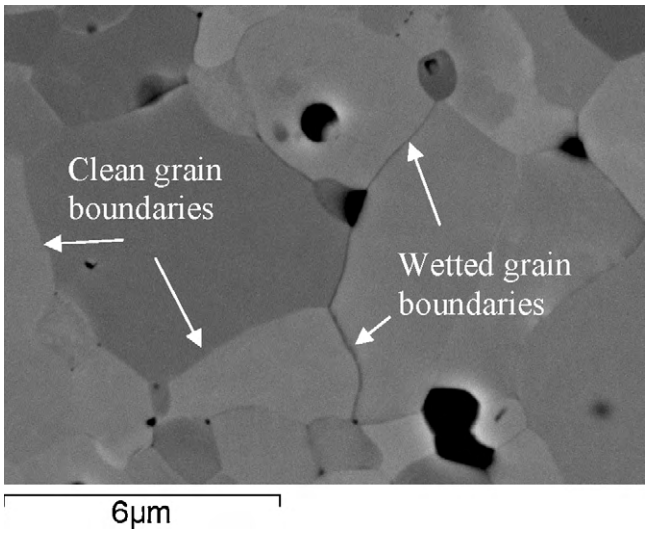

Fig. 4. Polished section of HBT3 showing low density grain boundary phases.

as reported elsewhere.[9,19,20] Small amounts of SiO_2, Si–O–C species and SiC were also detected (2–3%). Occasionally, large SiC agglomerations were observed in the microstructure, Fig. 2c. As previously reported,[23] during thermal treatment, $MoSi_2$ reacts with surface oxides, forming silica and other Mo–Si–B species which can be liquid at the sintering temperature. A possible reaction is:

$$MoSi_2 + B\text{–}Ospecies \rightarrow SiO_2 + Mo\text{–}B/Mo\text{–}Si\text{–}Bspecies \quad (1)$$

Once borides grains are depleted of their surface oxide, they can sinter by solid state and by liquid phase sintering mechanisms. The presence of a Carbon rich atmosphere favors the carbothermal reduction of SiO_2 into Si–O–C or SiC species, according to reactions such as:

$$SiO_2 + 3C \rightarrow SiC + 2CO(g) \quad (2)$$

TEM studies performed on borides doped with $MoSi_2$ showed that residual Mo–Si–B species can be found at triple points.[23] Residual wetting low density phases were also occasionally found at triple points.[23]

3.2.2. HBT3

X-ray diffraction spectrum showed in Fig. 1, pointed out the presence of crystalline HfO_2, and traces of hexagonal SiC. No $TaSi_2$ was instead detected. In agreement with the density measurements the microstructure showed a good level of densification (Fig. 3a–c), with a limited amount of closed porosity. The mean HfB_2 grain size was around 2–3 μm indicating that a significant grain coarsening occurred during sintering, in comparison with the HBM3 composite. This coarsening was

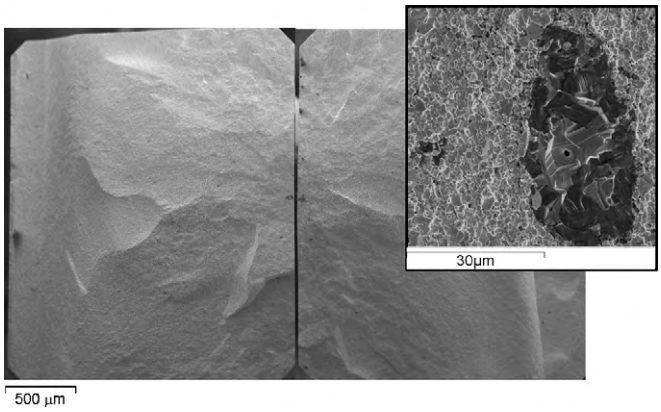

Fig. 5. Critical defect on the surface of HBM3 after strength test at room temperature (inset: enlarged view of the SiC critical defect).

certainly related to the higher sintering temperature of 2000 °C compared to 1900 °C of HBM3. As for HBM3, a significant fraction of HfO_2 was detected.[21] Residual SiC was also easily detected in the microstructure, with a percentage estimated through image analysis to be around 3%. The SiC phase is present in form of small rounded grains or as large SiC agglomerates, as illustrated in Fig. 3c. Identification of residual $TaSi_2$ in the microstructure was not possible due to the low amount and to overlapping of EDS signals collected from Hf, Ta and Si around 1.7 keV. Instead, it is apparent that HfB_2 grain boundaries are often but not always wetted by low density phases (Fig. 4). The black little pockets at the triple grain junctions are a mixed phase containing Hf, Ta, Si, B. According to previous findings on HfB_2–$TaSi_2$ composites,[21] during thermal treatment, $TaSi_2$ undergoes decompositions either reacting with B_2O_3 species or reacting with gaseous CO. Both these processes lead to release of Ta and formation of liquid Si or SiO_2-based phases. Possible reactions are:

$$3TaSi_2 + 2B_2O_3 = 2TaB_2 + Ta + 6SiO(g) \text{ favourable above } 1800\,^{\circ}C, \quad (3)$$

$$TaSi_2 + CO(g) = TaC + Si(l) + SiO(g) \text{ favourable above } 1100\,^{\circ}C \quad (4)$$

The most important result of $TaSi_2$ reaction with B_2O_3 is the oxygen removal from the boride particles and the formation of low density grain boundary phases, which promote mass transfer mechanisms and hence densification. The most important outcome of $TaSi_2$ reaction with CO is the formation of SiC deriving from carburization of Si. Released Tantalum or TaB_2 is instead hypothesized to enter in solid solution with HfB_2. Indeed the formation of solid solutions was assessed for HfB_2 composites

Table 2
Mechanical properties of the SPS-ed composites.

Sample	E (GPa)	ν	HV (GPa)	K_{Ic} (RT) (MPa m$^{1/2}$)	K_{Ic} (1500 °C) (MPa m$^{1/2}$)	σ (RT) (MPa)	σ (1200 °C) (MPa)	σ (1500 °C) (MPa)
HBM3	529	0.127	19.5 ± 0.8	4.4 ± 0.1	4.0 ± 0.4	760 ± 91	563 ± 37	483 ± 17
HBT3	539	0.115	20.9 ± 1.2	5.1 ± 0.2	4.9 ± 0.5	579 ± 44	344 ± 22	286 ± 33

Table 3
Mechanical properties of various HfB_2-based composites.

Samples (vol%)	E (GPa)	HV (GPa)	K_{Ic} (RT) (MPa $m^{1/2}$)	σ (RT) (MPa)	σ (1200 °C) (MPa)	σ (1500 °C) (MPa)
HfB_2 + 15 $MoSi_2$ (SPS)[9]	519	15.7 ± 0.8	3.8 ± 0.1	511 ± 119	–	573 ± 26
HfB_2 + 15 $MoSi_2$ (HP)[21]	530	20.6 ± 0.4	3.8 ± 0.1	742 ± 151	664 ± 28	548 ± 20
HfB_2 + 15 $TaSi_2$ (HP)[21]	528	21.9 ± 0.5	4.1 ± 0.1	698 ± 58	703 ± 24	597 ± 46

containing higher amounts of silicide[21] by SEM, TEM and X-ray diffraction analyses. Specific studies on densification behaviour of $TaSi_2$-doped composites are in progress and will be object of future publications.

3.3. Mechanical properties

The mechanical properties are reported in Table 2. Because the hardness of $TaSi_2$ (15.6 GPa)[24] is higher than $MoSi_2$ (12 GPa),[25] the $TaSi_2$-reinforced composites were harder than the $MoSi_2$-reinforced composites. Conversely, despite $MoSi_2$ has a higher stiffness than $TaSi_2$ (E = 425 GPa,[26] 360 GPa,[27] respectively) HBT3 stiffness was slightly higher than HBM3. It is very likely that conversion of $TaSi_2$ into a highly stiffness phase such as SiC had a positive influence on the composite elastic modulus. The ceramic doped with $MoSi_2$ had significantly higher values of strength both at room temperature and at high temperature. The room temperature flexural strength of HBT3 was mainly affected by the coarser microstructure, as evidenced by microstructural analyses. Fractographic analysis of specimens after strength tests at room temperature showed that in both the composites critical defects were mainly large SiC agglomerates. An example of such defects is reported in Fig. 5. An estimation of the critical defects size calculated using Griffith's law yields a value of 50 μm, which agrees very well with the actual size of SiC agglomerates as that presented in the inset of Fig. 5.

During the strength tests at 1200 °C the recorded load-displacement curves of HBM3 and HBT3 were linear up to fracture. At 1500 °C a slight departure from linearity was occasionally observed only for HBT3. It is very likely that softening of amorphous films along HfB_2 grain boundaries affected the high-temperature strength of this composite.

Despite HBT3 was about 24% less resistant than HBM3, it was about 16% tougher. An improvement of toughness by change of secondary phase from Mo- to Ta-disilicide was already observed for HfB_2- and ZrB_2-based composites containing 15 vol% $TaSi_2$.[21] It is worth noting that for both materials, fracture toughness did not change significantly when tested at 1500 °C in air.

Table 3 summarizes the mechanical properties of HfB_2-based materials containing 15 vol% of $TaSi_2$ or $MoSi_2$. It is apparent that for most properties, reduction of $MoSi_2$/$TaSi_2$ additions did not have significant effects, with few exceptions. One is the higher values of room temperature toughness displayed by HBT3 (Table 2), which may have been positively influenced by complete conversion of $TaSi_2$ to SiC. Conversely, the 1500 °C strength in air was generally higher for higher silicide content. This is an indication that glass formation can effectively blunt cracks leading to strength retention. Hence the decrease of the $MoSi_2$/$TaSi_2$ content from 15 to 3% led to a faster decrease of high-temperature strength.

4. Conclusions

HfB_2-based composites containing 3 vol% of molybdenum or tantalum silicide as sintering additives were fully densified by spark plasma sintering at 1900 and 2000 °C, respectively, thanks to the presence of liquid phases. The final microstructures were almost pore-free and with small grain size, 1 and 3 μm for $MoSi_2$- and $TaSi_2$-doped, respectively. The composites were hard (20–22 GPa) and stiff (530–540 GPa). The $MoSi_2$-doped composites had higher strength at room temperature (760 MPa) and at 1500 °C (480 MPa). $TaSi_2$ doping resulted in higher toughness, 5.1 MPa $m^{1/2}$. For both composites the fracture toughness tested at 1500 °C was not significantly different from the room temperature value.

Acknowledgement

The authors wish to thank C. Melandri for mechanical tests and G. Celotti for X-ray diffraction analyses.

References

1. Fahrenholtz WG, Hilmas GE. Refractory diborides of zirconium and hafnium. *J Am Ceram Soc* 2007;**90**:1347–64.
2. Opeka MM, Talmy IG, Zaykoski JA. Oxidation-based materials selection for 2000 °C + hypersonic aerosurfaces: theoretical consideration and historical experience. *J Mater Sci* 2004;**39**:5887–904.
3. Upadhya K, Yang JM, Hoffmann WP. Materials for ultrahigh temperature structural applications. *Am Ceram Soc Bull* 1997;**58**:51–6.
4. Clougherty, E. V., Kalishi, D., and Peters, E.T., Research and development of refractory oxidation resistant diborides. AFML-TR-68-190; 1968.
5. Gasch M, Elleby D, Irby EI, Beckam S, Gusman M, Johnson S. Processing properties and arc jet oxidation of hafnium diboride/silicon carbide ultra high temperature ceramics. *J Mater Sci* 2004;**39**:5925–37.
6. Opeka MM, Talmy IG, Wuchina EJ, Zaykoski JA, Causey SJ. Mechanical, thermal, and oxidation properties of refractory hafnium and zirconium compounds. *J Eur Ceram Soc* 1999;**19**:2405–14.
7. Wuchina E, Opeka M, Causey S, Buesking K, Spain J, Cull A, Routbort J, Guitierrez-Mora F. Designing for ultrahigh-temperature applications: The mechanical and thermal properties of HfB_2, HfC_x, HfN_x, and alpha Hf(N). *J Mater Sci* 2004;**39**:5939–49.
8. Silvestroni L, Sciti D. Effect of $MoSi_2$ addition on the properties of Hf- and Zr-B_2 composites produced by pressureless sintering. *Scripta Mater* 2007;**57**:165–8.
9. Sciti D, Silvestroni L, Bellosi A. Fabrication and properties of HfB_2–$MoSi_2$ composites produced by hot pressing and spark plasma sintering. *J Mater Res* 2006;**21**:1460–6.

10. Shen Z, Zhao Z, Peng H, Nygren M. Formation of tough interlocking microstructures in silicon nitride ceramics by dynamic ripening. *Nature* 2002;**417**:266–9.
11. Munir ZA, Anselmi-Tamburini U, Ohyanagi M. The effect of electric field and pressure on the synthesis and consolidation of materials. *J Mater Sci* 2006;**41**:763–77.
12. Nygren M, Shen Z. Novel assmeblies via spark plasma sintering. *Sil Ind* 2004;**69**:211–8.
13. Groza JR, Zavaliangos A. Sintering activation by external electrical field. *Mater Sci Eng* 2000;**A287**:171–7.
14. Groza JR, Garcia M, Schneider JA. Surface effects in field assisted sintering. *J Mater Res* 2001;**16**:286–92.
15. Anselmi-Tamburini U, Gennari S, Garay JE, Munir ZA. Fundamental investigations on the spark plasma sintering/synthesis process. II: Modelling of current and temperature distributions. *Mater Sci Eng* 2005;**A 394**: 139–48.
16. Anselmi-Tamburini U, Kodera Y, Gasch M, Unuvar C, Munir ZA, Ohyanagi M, Johnson SM. Synthesis and characterization of dense ultra-high temperature thermal protection materials produced by field activation through spark plasma sintering (SPS). I: Hafnium diboride. *J Mater Sci* 2006;**41**: 3097–104.
17. Basu B, Raju GB, Suri AK. Processing and properties of monolithic TiB_2 based materials. *Int Mater Rev* 2006;**51**:352.
18. Guo SQ, Kagawa Y, Nishimura T. Mechanical behavior of two-step hot-pressed ZrB_2-based composites with $ZrSi_2$. *J Eur Ceram Soc* 2009;**29**:787.
19. Sciti D, Silvestroni L, Nygren M. Spark plasma sintering of Zr- and Hf-borides with decreasing amounts of $MoSi_2$ as sintering aid. *J Eur Ceram Soc* 2008;**28**:1287–96.
20. Sciti D, Guicciardi S, Nygren M. Densification and mechanical behavior of HfC and HfB_2 fabricated by spark plasma sintering. *J Am Ceram Soc* 2008;**91**:1433–49.
21. Sciti D, Silvestroni L, Celotti G, Melandri C, Guicciardi S. Sintering and mechanical properties of ZrB_2–$TaSi_2$ and HfB_2–$TaSi_2$ ceramic composites. *J Am Ceram Soc* 2008;**91**:3285–91.
22. Munz DG, Shannon Jr JL, Bubsey RT. Fracture toughness calculation from maximum load in four point bend tests of chevron notch specimens. *Int J Fract* 1980;**16**:R137.
23. Silvestroni L, Kleebe HJ, Lauterbach S, Müller M, Sciti D. Transmission electron microscopy on Zr- and Hf-borides with $MoSi_2$ addition: densification mechanisms. *J Mater Res* 2010;**5**:828.
24. Schultes G, Schmitt M, Goettel D, Freitag-Weber O. Strain sensitivity of TiB_2, $TiSi_2$, $TaSi_2$ and WSi_2 thin films as possible candidates for high temperature strain gauges. *Sens Actuators A* 2006;**126**: 287–91.
25. Sciti D, Guicciardi S, Bellosi A. Microstructure and properties of Si_3N_4–$MoSi_2$ composites. *J Ceram Proc Res* 2002;**3**:87–95.
26. Nakamura M, Matsumoto S, Hirano T. Elastic constants of $MoSi_2$ and WSi_2 single-crystals. *J Mater Sci* 1990;**25**:3309–13.
27. Chu F, Lei M, Maloy SA, Petrovic JJ, Mitchell TE. Elastic properties of C40 transition metal disilicides. *Acta Mater* 1996;**44**:3035–48.